Scanning Electron Microscopy

Volume 1985
Number 1 *1985*

Article 1

11-16-1984

Digital Processing of Electron Energy Loss Spectra and Images

R. D. Leapman
National Institutes of Health, Bethesda

K. E. Gorlen
National Institutes of Health, Bethesda

C. R. Swyt
National Institutes of Health, Bethesda

SCANNING ELECTRON MICROSCOPY/1985/I (Pages 1-13)
SEM Inc., AMF O'Hare (Chicago), IL 60666 USA

DIGITAL PROCESSING OF ELECTRON ENERGY LOSS SPECTRA AND IMAGES

R.D. Leapman*, K.E. Gorlen and C.R. Swyt

National Institutes of Health, Bethesda, MD 20205

(Paper received March 26 1984, Completed manuscript received November 16 1984)

Abstract

Processing in electron energy loss spectroscopy involves both data acquisition and analysis. The interface of an analytical electron microscope to a laboratory computer with a satellite microcomputer dedicated to data acquisition results in a system with a high degree of flexibility. In spectrum acquisition, channels may be selected around specific core edges, or dwell times may be varied continuously as a function of energy loss to reduce the dynamic range of the signal. Data transfer to the host computer allows further analysis such as the removal of plural scattering by spectral deconvolution. Elemental maps and line-scans can be recorded with real-time processing of energy loss data at each pixel. Images may be analyzed to provide quantitative information by means of pixel intensity histograms. If parameters for the background are stored at each pixel, the image data may sometimes be further processed to improve the signal-to-noise ratio.

KEYWORDS: Electron Energy Loss Spectroscopy, Digital Processing, Computer Interface, EELS Acquisition System, Spectrum Analysis, Line-scan, Background Subtraction, Elemental Mapping.

*Address for correspondence:
R.D. Leapman
Biomedical Engineering and Instrumentation Branch,
Bldg. 13, Rm 3W13
National Institutes of Health
Bethesda, Maryland 20205
Phone No. 301 496-4426

Introduction

Efficient processing of data obtained from inelastic scattering in the electron microscope constitutes an essential part of electron energy loss spectroscopy (EELS). The processing can be broadly separated into two categories: real-time acquisition and off-line analysis. Data acquisition can range in complexity from simple analog control of an electron spectrometer to full digital control of not only the spectrometer but also the scanning transmission electron microscope (STEM). Data analysis generally involves the use of a laboratory computer or a special-purpose commercial EELS system.

In standard acquisition of energy loss spectra, single scattered electrons are detected as digital pulses. This output must often be fully exploited to detect very weak signals, obscured by background noise, such as occur in core edge microanalysis or in energy loss fine structure [6,21]. It has been found convenient to take advantage of multichannel analyzer (MCA) systems that were originally intended for use in energy dispersive x-ray spectroscopy [13,27]. The MCA can be readily adapted to count single electrons in EELS, to provide a voltage ramp for the spectrometer excitation, and to display resulting spectra. Moreover, the commercial systems are equipped with microprocessors that are capable of limited analysis and quantification of EELS spectra. Although advances in computer technology are increasing the power of commercial EELS systems, there may still be some advantage in transferring data to a laboratory computer, which can provide a more flexible environment for program development and data analysis.

However, the experimenter may wish to collect spectra with increased control. It may be useful, for example, to vary the dwell-time per channel or to compensate for the high dynamic range of the signal [1,7,16,20]. Digital acquisition is also desirable in EELS elemental imaging to increase flexibility and to facilitate real-time processing [19,20]. Requirements for computer hardware, software and microscope interface obviously depend on the level of control that is needed. At the present state-of-the-art, digital acquisition of EELS images or line-scans depends heavily on specially designed hardware and software [19,20,30]. The quantity and rate of incoming data

for imaging lead to minimum requirements for storage and computer speed. For example the system that we describe has some 100 M Byte of disk storage and can process data at a rate of $2x10^5$ floating point operations per second (200 k FLOPS). There are additional requirements for the analysis of resulting data. Thus, for example, it may be necessary to incorporate a digital array processor so that simple arithmetic operations may be carried out efficiently on images containing as many as 10^5 pixels.

The aim of this paper is to demonstrate how the capabilities of EELS can be significantly enhanced by digital processing. We shall choose examples from the system currently in use in our laboratory and the emphasis will mainly be on applications. Clearly, design of a digital data acquisition system involves a considerable effort in the computer interface and in software development. For a more complete discussion of these aspects the reader is referred to other published work [3,19,20,29,30,43].

Acquisition Systems

An example of a simple EELS acquisition system for use with an analytical electron microscope is shown in Fig. 1. A commercial MCA system, in this case a Kevex 7000, provides a voltage ramp which drives a current supply to control the excitation in the coils of a 90° magnetic sector spectrometer. The spectrometer disperses the inelastically scattered electrons according to their energy loss and focusses them in a plane containing a slit, positioned perpendicular to the dispersion direction. A spectrum is recorded by varying the magnetic field while electrons passing through the slit are detected with a scintillator and photomultiplier. The dwell-time per channel, the range of energy losses and the number of sweeps through the spectrum may be controlled from the Kevex 7000 keyboard. Digital pulses originating from individual fast electrons are preamplified and discriminated before entering a counter (multichannel scaler). The counts are stored in their appropriate channels (0-1024) and are registered on the MCA display. Spectra may be transferred rapidly to a larger computer, in this case a Digital Equipment Corporation PDP 11/60, across a standard data bus (DEC unibus).

Greater control of data acquisition can be achieved by means of a specially programmed computer interfaced to the microscope [3,19,20,29,30,43]. Fig. 2 shows schematically part of a system that has been developed in our laboratory to control a Hitachi H700 H analytical electron microscope. The system as a whole, which has been discussed elsewhere [20], is designed to acquire a number of signals including x-ray, axial bright field and annular dark field STEM, but Fig. 2 shows only that part concerned with the energy loss signal. A satellite computer (LSI 11/23) controls data acquisition after appropriate software is downloaded from the host computer (PDP 11/60) that is connected to the satellite via a high speed direct memory access link. Use of a separate processor to acquire data removes real-time load from the host so that it is free to handle other operations. Digital-to-analog converters (DACs) provide the voltages necessary for the interface. The satellite controls both the magnet excitation and the voltage on electrostatic deflection plates situated just before the analyzing slit of the spectrometer [18]. The satellite can synchronize spectrum acquisition with scan of the electron probe at the sample in STEM mode to produce an EELS image. Deflection of the spectrum through control of the magnetic field provides an energy loss offset that is nearly linear over a range in excess of 0-2 keV at beam energies from 75 to 200 keV. Response of the energy loss offset to the changing magnet excitation is too slow for use in imaging, but EELS mapping may be performed by varying the electrostatic field between the deflection plates. The deflection plate voltage can be adjusted at a rate of some 10^5 V/s to provide rapid response over 1 keV of energy loss. The satellite uses a timer to enable a 32-bit counter for a precise time interval. When the interval has elapsed, the timer interrupts the satellite which reads the number of counts accumulated at the energy and saves the value in a buffer. The magnet excitation, the deflection plate voltage or both of these can then be readjusted and the timer restarted to repeat the process. A counter with 32-bits is required as a

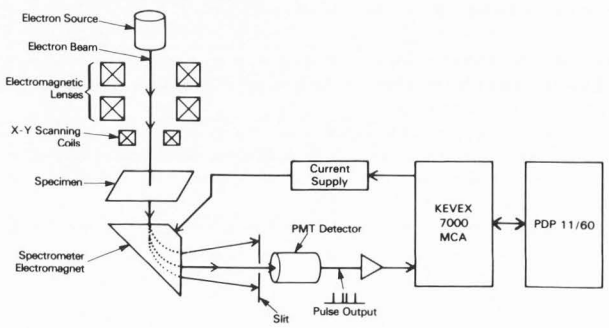

Fig. 1 Schematic diagram of analytical electron microscope with energy loss spectrometer, controlled by commercial MCA system linked to laboratory computer.

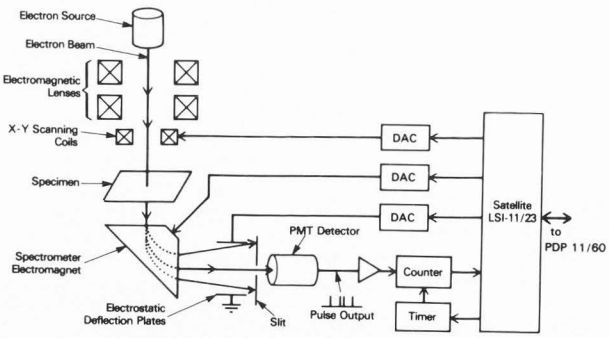

Fig. 2 Schematic diagram of analytical electron microscope with energy loss spectrometer, interfaced to laboratory computer via a satellite that controls data acquisition [20].

consequence of the wide dynamic range of intensities that is encountered in EELS. The signal is converted to a floating point number in the host computer because floating point numbers can be processed more rapidly than 32-bit integers in our system. After acquisition, the data is transferred to the PDP 11/60 where it can be stored on disk and processed. Spectra can be displayed by transfer to the MCA across the data bus. Images are transferred to a DeAnza IP 6400 image display system, that is also linked to the host computer.

Data acquisition is controlled through programs selected from menus displayed on a terminal. The menus contain tables of parameters and commands that specify the acquisition and which can be updated, saved and executed. This software is discussed by Gorlen et al. [20].

The system outlined above is designed for serial detection of scattered electrons. Although serial recording is the most widely adopted method, it is intrinsically inefficient since only a single spectral channel is recorded at any one time. Recently there has been considerable interest in the use of much more efficient position-sensitive parallel detectors, that can collect a large number of spectral channels simultaneously. The best suited devices at present appear to be the linear photodiode array [15,25] and the silicon intensified target (SIT) vidicon [40]. It is generally advantageous to use an indirect exposure method to limit radiation damage in the detector. Fast electrons first strike a phosphor in the spectrometer image plane and the resulting photon distribution is then focussed by light optics on to the detector. Parallel collection of EELS data and the signal processing that is required have recently been discussed by Egerton [15]. Light incident on a diode array generates electrons and holes whose number is measured by the rate at which diode discharge occurs. After a given integration time the amount of applied charge required to recharge each diode can be monitored. This is read out serially as a video signal by appropriate timing and amplification circuitry. In order to store a spectrum the video signal is digitized and fed into an MCA. This requires synchronization of the MCA channels with the array read-out, which can be supplied by timing pulses from the diode array. Alternatively, it may be advantageous to provide all timing pulses for the diode array from the MCA. Egerton has discussed the processing that is necessary to remove artifacts due to the parallel detector [15]. Variation in diode sensitivity may under some circumstances be corrected by simple normalization procedure. This involves dividing the data by the response characteristic measured when the zero-loss beam is scanned across the array. The normalization procedure is not valid when the detector sensitivity and the scattered electron distribution vary in a direction perpendicular to the dispersion direction. In these cases, Shuman et al. [41] have demonstrated that channel-to-channel gain variations may be eliminated by displacing the spectrum across the detector by ±1 channel. Subtraction of twice the undisplaced spectrum from the sum of the two displaced ones, produces a result equivalent to the second derivative but with channel-to-channel noise removed.

Spectrum acquisition

A typical core edge spectrum acquired from a biological sample under digital control is shown in Fig. 3. The dwell time per channel was 100 ms and the spectrum was collected over a 500 eV range of energy loss starting at 200 eV. Although the result is similar to that obtainable with a commercial EELS system digital control does simplify magnet calibration. In our system a trial spectrum is acquired over a range of typically 0-1000 eV with the most recent set of calibration parameters, which are given in terms of the DAC volts per eV of energy loss and the zero-loss offset. The resulting spectrum is then transferred to the MCA and known

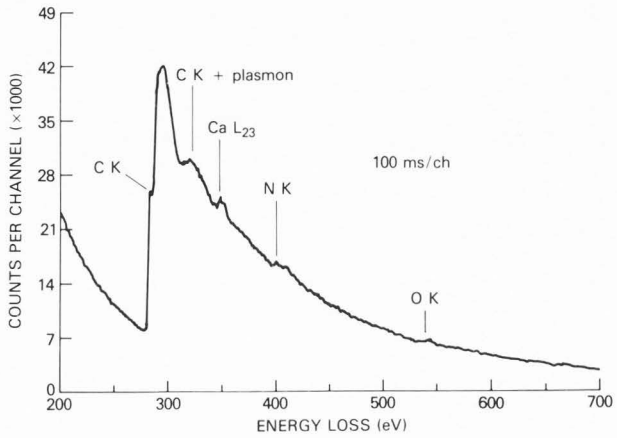

Fig. 3 Electron energy loss spectrum in core edge region from embedded biological section of mineralized tissue, recorded in 50 s.

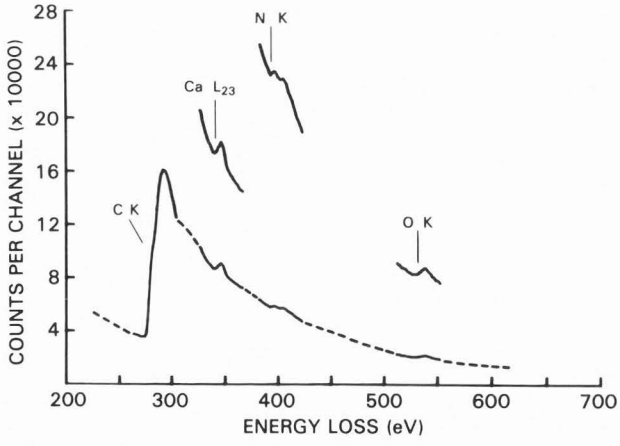

Fig. 4 Electron energy loss spectrum acquired under computer control in segments confined to ± 20 eV of the C K, Ca L_{23}, N K and O K edges. Counting times per channel for these edges were 0.1, 0.2, 0.4 and 0.4 s respectively. Raw data in upper segments. Data in lower segments scaled according to counting time. Dashed curve indicates region of spectrum not collected.

features such as the carbon and oxygen K edges are marked with cursors on the display. New parameters are computed so the next spectrum acquired is correctly calibrated as demonstrated in Fig. 3.

Serial recording can be made more efficient by acquiring the spectrum in segments each extending over an energy range containing only particular edges of interest. Different dwell times per channel can also be selected for each segment to achieve the required counting statistics for specific edges. In the present system the scanning time for the magnetic field requires about 2 s delay per keV of spectrum before the field stabilizes. The satellite automatically pauses after slewing the spectrometer excitation current between spectrum segments to stop data acquisition while the magnetic field is still changing.

Fig. 4 shows a spectrum in the neighborhood of the carbon K, calcium L_{23}, nitrogen K and oxygen K edges from the same sample that was analyzed in Fig. 3. The spectrum consisting of 160 channels was recorded in 45 s with longer dwell times for the weaker core edges as indicated. During the acquisition the spectrum was scanned ten times past the detector. Multiscanning is useful if there is sample drift or damage, because the whole spectrum is characteristic of the area irradiated, rather than different channels in the spectrum corresponding to different conditions. The unconnected segments of the spectrum in Fig. 4 are the measured counts; the lower segments, joined by dashed lines, are the measured counts scaled according to the dwell-time for the carbon K edge to give a continuous spectrum.

In the core loss region the count rate approximately follows an inverse power law [10] being proportional to E^{-r} where E is energy loss and r is a constant typically in the range 3 to 4. Under computer control the counting time can be incremented at each channel to compensate for this decrease in intensity and to produce a step-like spectrum [40]. The result is easier to display since it covers a smaller dynamic range. Also the spectrum has nearly constant signal-to-noise ratio, making high energy edges easier to discern. The spectrum in Fig. 5 was acquired with the counting time determined by the formula

$$t_i = 300\left[\frac{E_i}{832}\right]^3 \qquad (1)$$

where the counting time for channel i, t_i, is in milliseconds and the energy of channel i, E_i, is in electron volts. The sample was the same as for Fig. 3 but the calcium, nitrogen and oxygen core edges are more visible.

Spectrum analysis

Analysis of spectra can be carried out either with a commercial MCA system or with a larger computer linked to the MCA which provides a convenient display. For example, the Kevex 7000 in our system is connected via the DEC unibus to the PDP 11/60 computer (Fig. 1). Special software must be written to access the MCA memory. Once this is provided "read" and "write" subroutines can be incorporated into programs written in widely-used

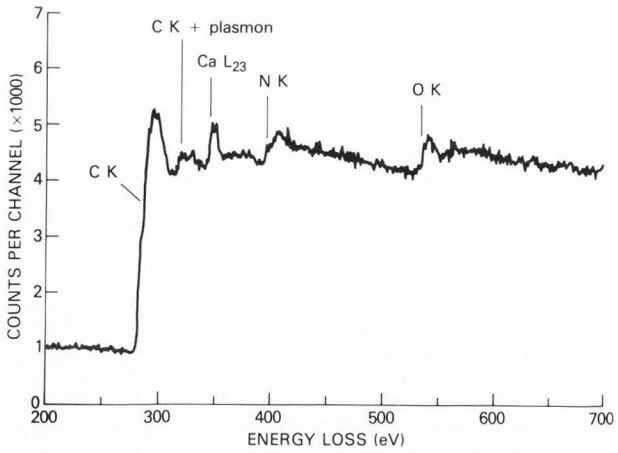

Fig. 5 Spectrum produced by using counting time that increases with cube of energy loss. Dynamic range is significantly reduced compared with Fig. 3.

languages such as FORTRAN and PASCAL. Our PDP 11/60 has a 232 k Byte MOS memory (metal oxide semiconductor) and two 67 M Byte disks capable of storing hundreds of thousands of spectra. The computer uses a flexible DEC operating system (RSX11) with a mathematical and scientific subroutine library.

Certain analyses can be readily performed with software running in a commercial system. Examples include: Linear least squares estimation of the background intensity for core edges [13]; calculation of ionization cross sections based on the hydrogenic model [12]; and quantitation schemes for elemental microanalysis [11,28]. Other analyses require the increased speed, memory and flexibility of a larger computer. It may be necessary to write a new program for a special application, or to use procedures such as the fast Fourier transform (FFT), which often cannot be executed rapidly on a small system. Examples of more sophisticated analyses include: derivation of the real and imaginary parts of the dielectric constant from the energy loss function by Kramers-Kronig analysis [9]; derivation of the local atomic environment from extended energy loss fine structure (EXELFS) [32]; derivation of the single scattering distribution for valence electron excitations [2,26]; and deconvolution of core edge spectra to remove plural scattering [17,33,37,44]. We shall discuss here only the last of these procedures in order to demonstrate the type of analysis that is possible with a flexible system.

Plural scattering becomes very important when the sample thickness approaches the total mean free path for inelastic scattering, which is typically only a few tens of nanometers at 100 keV beam energy. Core edges are therefore complicated by the occurrence of extra peaks arising from an inner shell plus one or more valence excitations. For energy losses above some 200 eV, where the pre-edge background can be subtracted with the well-known inverse power law [10], it has been shown that the single-scattering distribution for core edges can

be obtained by a deconvolution procedure [17,33,37,44]. If L(E) is the low loss spectrum and C(E) is the measured core loss spectrum after background subtraction, then the Fourier transform of the single-scattering core edge distribution is given by,

$$\hat{S}(\hat{E}) = \frac{\hat{C}(\hat{E})}{\hat{L}(\hat{E})} \qquad (2)$$

where ^ denotes Fourier variable.

S(E) can be recovered by an inverse Fourier transform provided the result is reconvoluted by a normalized instrumental resolution function $I_o(E)$ in order to truncate the high frequency Fourier coefficients and to prevent noise amplification.

$$S(E) = F.T.^{-1}\left[\frac{\hat{C}(\hat{E}).\hat{I}_o(\hat{E})}{\hat{L}(\hat{E})}\right] \qquad (3)$$

Fig. 6a shows the spectrum in the range 0 to 800 eV from a sample of titanium dioxide; it includes the low loss region as well as the titanium and oxygen core edges. Several peaks are visible above the Ti L_{23} edge (455 eV) and these cause confusion in the vicinity of the oxygen K edge (532 eV). Fig. 6b shows the measured core edge intensity after background subtraction and the computed single scattering distribution obtained from Eq. (3). A significant change in spectral shape is apparent; the intensity above the Ti L_{23} edge threshold resonance is reduced; and the oxygen K edge is much more clearly visible. In fact it is now possible to attempt quantitative analysis on the single-scattering distribution despite the proximity of the two edges. The deconvolution involves four FFTs on spectra containing 1024 channels. The total computation time on the PDP 11/60 system was about 5 s, including the time necessary to read the spectra and to write the single scattering distribution back into the MCA. The code was written in FORTRAN and called a standard DEC subroutine to perform the FFT.

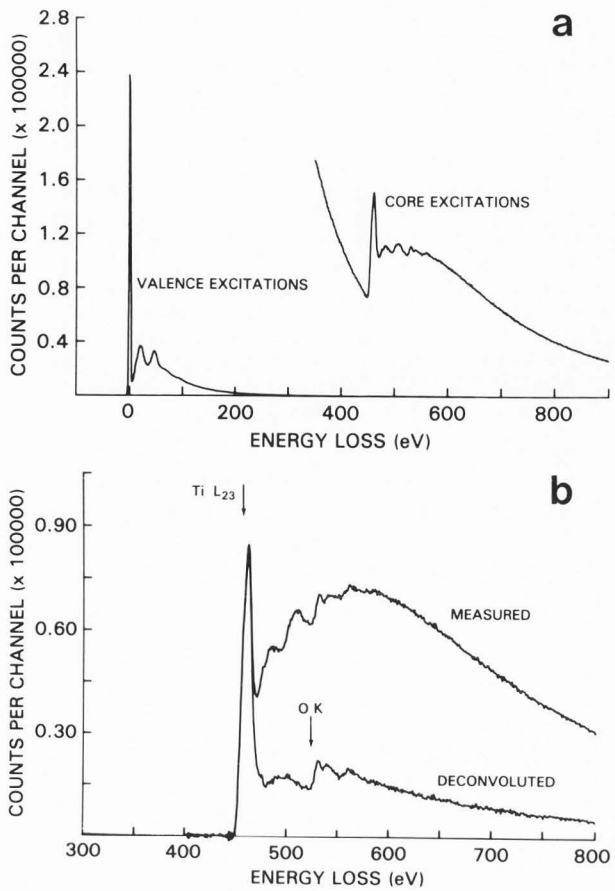

Fig. 6. (a) Spectrum from film of titanium dioxide showing zero loss, valence and core excitations. Plural scattering is apparent in structure above Ti L_{23} edge (455 eV).

(b) Measured and deconvoluted spectrum above Ti L_{23} edge after background subtraction. Removal of plasmon peaks enhances visibility of oxygen K edge (532 eV) in deconvoluted spectrum.

Real-time processing in mapping and line-scans

Elemental mapping by EELS requires the acquisition of spectral data at each pixel in an image. The spectrum is often dominated by the non-characteristic background intensity which must be subtracted by an extrapolation procedure to yield the signal. If the inverse power law is valid, two parameters define the background. Therefore at least two channels are required below the core edge to estimate the background and one channel above the edge to obtain the characteristic signal, as has been discussed by Jeanguillaume et al. [23,24], Rez and Ahn [38] and Butler et al. [4]. In general there is an advantage in recording several channels around a core edge. The most efficient method would be parallel detection so that all scattered electrons carrying elemental information are collected [15,25,40,41]. Serial acquisition in EELS mapping is more straightforward and has been achieved with the system that we have already outlined in Fig. 2. The satellite computer allows for as many as 64 channels to be collected at each pixel from four different edges. The core edge energies, number of channels in the fitting regions and post-edge regions, together with their energy separations are selectable. Rapid control of the spectrum offset is performed by means of the electrostatic deflection plates. Data acquired at one pixel by the satellite is sent to the host (PDP 11/60) which fits the background and calculates the integrated edge counts while data is being acquired from the next pixel. The integrated pixel intensities are buffered and written on to disk periodically. In addition to the intensities, associated parameters, A and r, that are obtained in the processing may be stored on disk and used in further analysis [34]. During image acquisition

the spectrum and background fit at each pixel, obtained by linear least squares estimation, are continuously displayed on the MCA monitor. By observing the dynamically updated display, the user can deduce if drift is occurring or if the spectrum has an unexpected shape due to plural scattering. This real-time processing provides the operator with valuable feedback and interaction. For example if a certain core edge is not visible at the beginning of image acquisition, it may be decided to abort the acquisition and move to a different specimen area.

The time required to collect an image clearly depends on the elemental concentration and on the probe current. We have been able to use acquisition times in the range 10 to 1000 ms per pixel with a 1 nA probe current. These conditions require between 3 and 30 min. to record a 128 x 128 pixel map. On this time scale long-term spectrum drift (1 or 2 eV per minute in our system) can seriously affect image quality. Such instability can be corrected under computer control [30,38]. At

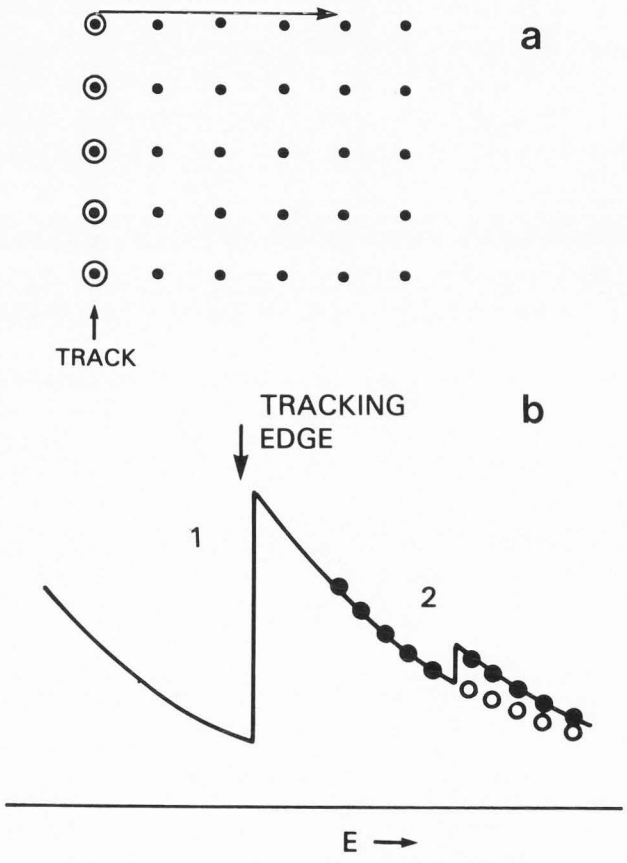

Fig. 7 (a) Scan-raster for EELS mapping with pixels at beginning of scan-lines selected for tracking a core edge to correct for spectrum drift.

(b) Channels at one pixel around a core edge (2) that is selected for elemental mapping. The edge (1) is tracked at the pixels indicated in (a).

the beginning of each scan line a spectrum is collected within ± 30 channels of a core edge that is present throughout the entire image. The maximum gradient of the smoothed acquired spectrum computed in the satellite gives the edge energy and the electrostatic voltage offset is adjusted accordingly. To eliminate the effects of noise the drift compensation is damped by allowing a maximum correction between scan lines. In biological samples it is convenient to track the carbon K edge. Fig. 7a is a schematic diagram of the scan-raster and Fig. 7b indicates how the edge-tracking is performed on edge 1 while an element is mapped with edge 2.

Figs. 8a and 8b are aluminum K edge (1560 eV) and silicon k edge (1838 eV) maps respectively that were obtained from an ion-thinned metal-ceramic composition consisting of silicon carbide grains in an aluminum matrix. A 200 eV fitting window, a 100 eV integration window and a total of 10 channels were selected for each edge. The aluminum image shows the presence of the matrix whereas the silicon image clearly indicates the carbide phase. The images were acquired concurrently at 200 keV beam energy in 16 min and contained 128 x 128 pixels.

It is also useful to acquire elemental profiles across a line in the sample [38]. This can be achieved in the system under consideration by defining a target area containing only one line. As with image acquisition, the satellite can lock-on to a dominant core edge at the first pixel so that the energy loss scale offset is automatically calibrated. Fig. 9 shows the distribution of calcium and nitrogen along a line in a sample of mineralizing enamel. The satellite locked-on to the carbon K edge (285 eV) while the calcium L_{23} (348 eV) edge and the nitrogen K edge (400 eV) were used to obtain the elemental profiles concurrently. A bright field digitized STEM image with 256 x 256 pixels was first recorded in a few seconds to provide a reference for the line target. Then 256-point elemental distributions of calcium and nitrogen were acquired in 100 s. Advantages of the line-scan are the quantitative graphical display of elemental concentrations and the much reduced time needed to collect line rather than image data.

A parallel detection system could in theory reduce image acquisition time in STEM, perhaps by over an order of magnitude. Elemental maps containing 10^5 pixels might then usefully be recorded in a few minutes. As we mentioned, Shuman et al. [41] have found that channel-to-channel noise can be eliminated by deflecting the spectrum across the parallel detector and reading the result several times at each pixel. The minimum time interval required to read out the array would therefore be an important factor in realizing rapid EELS imaging in STEM. However even with the same acquisition time as for serial collection, detection limits will be reduced with parallel detection.

It should be added that energy selected images have been recorded in the conventional transmission electron microscope (CTEM) by means of SIT vidicons or television camera tubes, which function as two dimensional parallel detection devices. Rust and

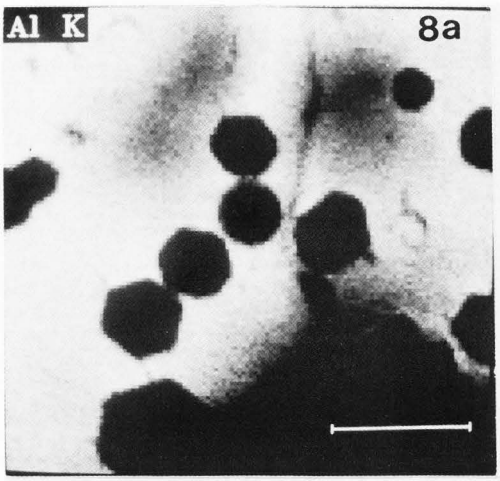

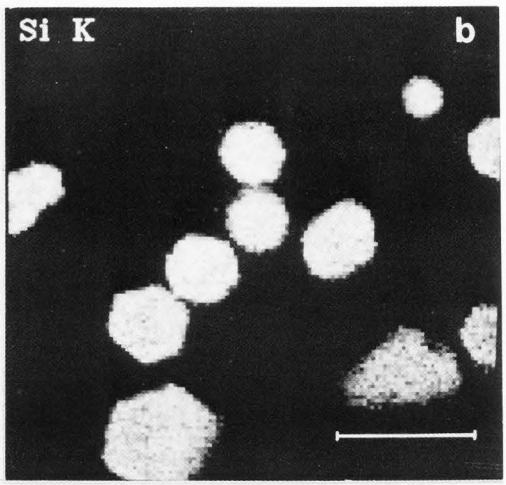

Fig. 8. EELS images containing 128 x 128 pixels recorded concurrently from metal-ceramic composite. (a) Aluminum K edge (1560 eV) and (b) silicon K edge (1838 eV). Bar = 0.5μm.

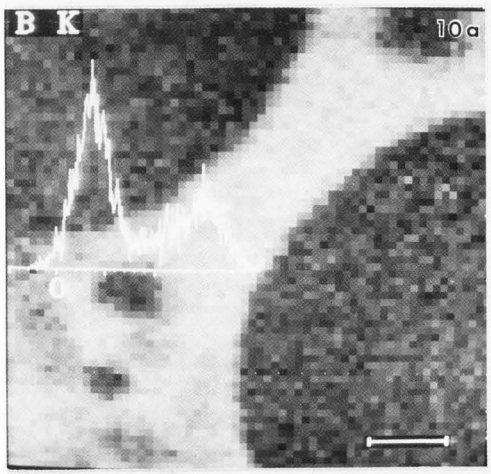

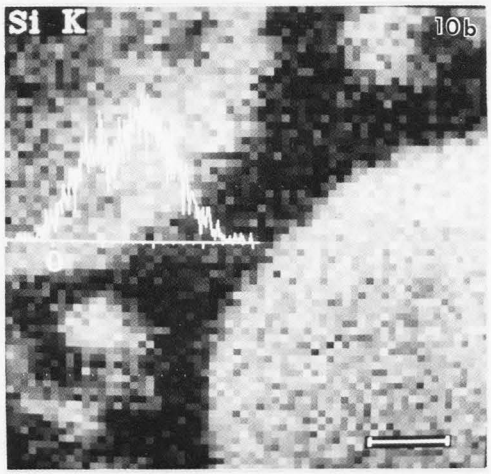

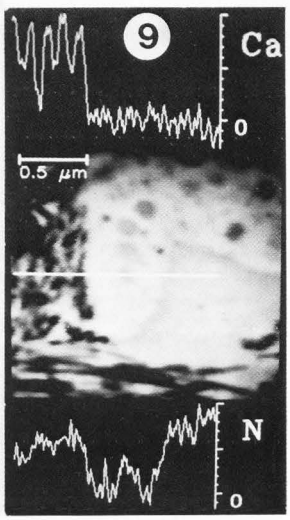

Fig. 9. Distribution of calcium and nitrogen along a line in a section of mineralizing enamel measured under computer control. Position of line on digitized bright-field CTEM micrograph is indicated. Notice calcium containing enamel crystallites on left side of image with underlying nitrogen-rich protein matrix. Nitrogen also occurs at right side of image in protein matrix that is free of calcium mineralization. Length of line is 2.0 μm.

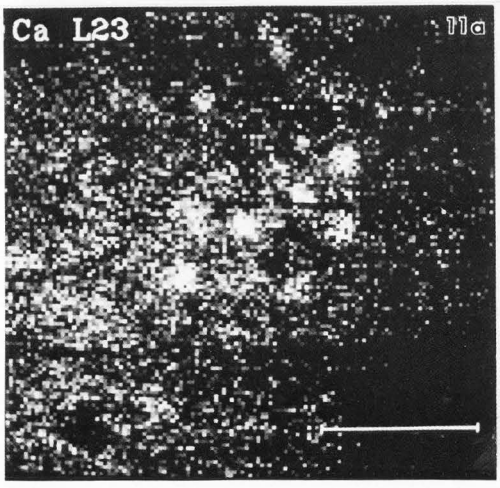

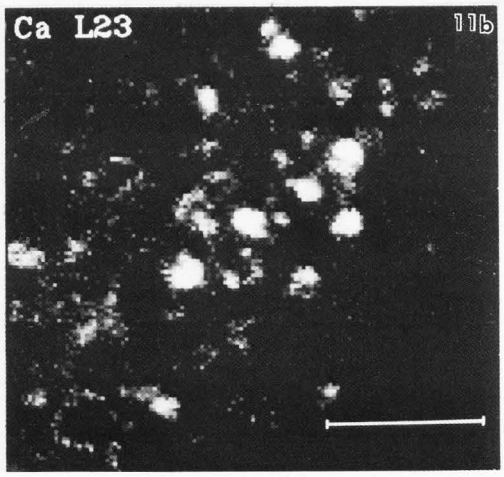

Fig. 10. EELS images with 64 x 64 pixels from borate-silicate glass. (a) Boron K edge (192 eV) and (b) Silicon K edge (1838 eV). Also shown are intensity histograms calculated in less than 10s with the use of an array processor in a DeAnza IP6400 display system [20]. The histograms show relative amounts of boron and silicon in the two phases. Bar = 0.1 μm.

Fig. 11. EELS calcium L_{23} map from mineralizing bone tissue section, (a) Two parameters, A and r, were fitted to extrapolate background intensity. (b) Calcium distribution obtained by fitting only one parameter, A, for the background. The parameter, r, was set equal to the mean r for the whole image. Bar = 1.0 μm.

Krahl [39] have used an omega-filter to select the energy loss and a camera tube situated at the final image plane of the microscope. The digitized sequential output of the vidicon was recorded in a TV image storage unit linked to a computer. Shuman and Somlyo [42] have used a magnetic sector spectrometer situated below the microscope projection chamber. A magnetic lens after the sector forms a magnified real image that is selected in energy by a slit in the dispersion plane. The filtered image is projected on to a phosphor and the resulting photon distribution can be further magnified by light optics before passing into the vidicon. Such electronically recorded EELS images may be compared with those recorded photographically with a Castaing-Henry filter by Ottensmeyer and Andrew [35]. In this case the data must be digitized by a densitometer. Parallel image collection in the CTEM is generally faster than serial collection in the STEM because of the higher available probe current. However, in terms of radiation damage, STEM has the advantage when the spectrum is recorded in parallel because of the higher detection efficiency. It is also more satisfactory to process EELS images recorded in the STEM because of the existence of reliable spectral data at each pixel.

EELS image analysis

In the analysis of energy loss images, procedures are necessary to manipulate data, to obtain quantitative information, and to optimize the signal-to-noise ratio. In the system we have been discussing, functions for scrolling, zooming and contrast enhancement have been implemented in a DeAnza IP 6400 image display system. This device is equipped with four 512 x 512 x 8 bit image channels, three of which can be displayed in color and one in monochrome. It is also equipped with a graphics overlay channel. Use is made of a digitizing tablet and stylus, which is tracked by a cursor on the display. With the cursor it is possible to select various options contained in a menu overlaid on the displayed image, as described Gorlen et al. [20].

One example of basic image analysis that has been implemented is the intensity histogram for an EELS map [20]. A region of an image is outlined on the display and a histogram is computed in less than 10 s by means of an array processor integrated into the DeAnza system. Fig. 10 shows 64 x 64 pixel boron K and silicon K edge images acquired separately in 6 min and 12 min respectively with the real-time background subtraction procedure described above. The sample was a borate-silicate glass prepared by ion-thinning. A 40 eV window was used to fit the background below the boron edge and a 20 eV window above the edge to obtain the integrated core loss signal. For silicon the pre-edge window was 80 eV and the post-edge window 40 eV. Intensity histograms reveal the relative concentrations of these elements in the two phases that are present. The concentration of boron in the spherical phase is approximately one-quarter that in the surrounding matrix (Fig. 10a), whereas the silicon concentration is twice as much in the spheres than in the volume outside (Fig. 10b).

It is useful to combine digital images arithmetically and this has been achieved in our system by the use of the DeAnza array processor to calculate the sum or difference of two 512 x 512 images in one video frame-time (1/30 s) and a quotient in less than 5 s [20]. The division function is important since it gives the ratio of two elemental distributions or allows a plural scattering correction to be made to a core loss map. The number of atoms n of an element in a pixel is approximately proportional to the core edge intensity, I_c, divided by the low loss intensity, I_l [11],

$$N \simeq \frac{I_c(\alpha,\Delta)}{I_l(\alpha,\Delta)\sigma_c(\alpha,\Delta)}\, d^2 \qquad (4)$$

where α is the collection angle, Δ is the integration window and $\sigma_c(\alpha,\Delta)$ is the appropriate partial cross section. $I_l(\alpha,\Delta)$ is the measured intensity including the zero loss peak up to energy loss Δ, and d is the pixel separation. This measurement must generally be obtained from a digitized analog current output since the count rate is too high for direct pulse counting. Eq. (4) accounts to first order for plural inelastic and elastic-inelastic scattering [11].

The division procedure can also be used in Z-contrast imaging [5,8,22] where a high angle annular dark field detector provides the elastic signal concurrently with the total inelastic signal from the energy loss spectrometer. The spectrometer slit is set to cover a range of valence excitations but to exclude the zero loss peak. Each signal is first digitized and the ratio of the elastic to inelastic image is computed. This ratio theoretically reflects the local mean atomic number of the sample. Not only is the result independent of sample thickness within the limits of single scattering [14] but also beam instabilities are eliminated in the ratio image.

There is a significant advantage in computing the ratio image digitally so that the individual dark field and inelastic images are saved. If the quotient is obtained with a ratio amplifier by analog means then the separate images are discarded.

In EELS image acquisition we can record not only the integrated core edges counts but also the parameters A and r derived from fitting the background to an inverse power law AE^{-r}. A more detailed analysis of the data is then possible [36]. Statistical errors may be significantly reduced if the shape of the background does not vary appreciably from pixel to pixel, so that a one-parameter fit can be used to model the background. Such an assumption is generally implicit in subtraction of the background image in energy selected micrographs recorded with a Castaing-Henry filter in the CTEM [35]. It is possible to predict under what circumstances the one-parameter fit should fail, by considering the relative magnitudes of systematic and statistical errors in the spectrum. If the spectral shape does vary due to plural scattering or compositional fluctuations, artifacts can arise in elemental distributions obtained with a one-parameter fit [23]. Another test is to inspect the "r-image" obtained by fitting two parameters. When structure

is observed caution must be exercised in fitting only one parameter for the background. If one parameter is justified a mean value of r over the whole image ($\bar{r}$) can be computed and a corrected value A' for the parameter A may be obtained at each pixel from the stored values of A and r [31]. If the pre-edge fitting window extends over N channels from energy E_1 to energy E_N, then,

$$A' = A(E_1 E_N)^{(\bar{r}-r)/2} \quad (5)$$

The correction to the pixel intensity obtained from the two-parameter fit is then found by summing the quantity (AE^{-r}-$A'E^{-\bar{r}}$) over the post-edge window.

This procedure is illustrated in Figs. 11a and 11b which show the calcium distribution in a section of mineralizing bone tissue. Fig. 11a is the image at the calcium L_{23} edge (348 eV) after real-time processing involving the two parameter fit to the background. Five pre-edge channels with 5 eV separation and 5 post-edge channels with 3 eV separation were selected. The acquisition time for 128 x 128 pixels was 16 min. Fig. 11b shows the image derived from the same raw data but with a one-parameter fit. A significant reduction in noise is apparent and additional structure is observed which was confirmed by the occurrence of a calcium edge in the spectrum. This program for recalculating the EELS image did not utilize the DeAnza array processor so the execution time of 2 min was longer than for the image division program. However, it is important to appreciate the assumptions that are made in this type of processing to avoid the possibility of artifacts.

Summary

We have shown that processing of EELS data plays an important role in the acquisition and analysis of spectra and images. An acquisition system has been described, that incorporates a laboratory computer and a dedicated satellite computer to control an analytical electron microscope. Data can be processed digitally in real time so it is possible to correct for spectrometer drift and to provide valuable feedback to the experimenter during acquisition of elemental distributions. Spectra may be analyzed off-line in the host computer with programs written in standard languages. Results are conveniently displayed on a commercial MCA system linked to the computer. Images may be handled by use of a digital display system equipped with an array processor, allowing procedures such as intensity histograms to be performed very efficiently. We have seen that digital processing provides the flexibility to exploit the information contained in the energy loss signal.

Acknowledgments

The authors are indebted to C.E. Fiori and C.C. Gibson for work on the computer controlled analytical electron microscope, and to J.S. Del Priore, L.K. Barden, A.K. Kochhar and S.M. Orlow for writing software for the system. They thank Dr. S. Nutt (Arizona State University, Tempe) for the silicon carbide-aluminum composite sample, Dr. A.E. Zaki (University of Illinois, Chicago) for the mineralizing enamel sample, and Professor R.F. Egerton (University of Alberta, Edmonton) and Dr. P. Taylor (Whiteshell Nuclear Research Establishment, Manitoba) for the borate-silicate glass sample.

References

1. Batson, P.E. (1979). Digital data acquisition of electron energy-loss intensities. Ultramicroscopy 3, 367-371.

2. Batson, P.E., Silcox, J. (1983). Experimental energy loss function, Im $(-1/\varepsilon(q,\omega))$, for aluminium. Phys Rev. B27, 5224-5239.

3. Batson, P.E., Trafas, G. (1982). The IBM computer-STEM system. Ultramicroscopy 8, 293-300.

4. Butler, J.M., Watari, F., Higgs, A. (1982). Simultaneous collection and processing of energy-filtered STEM images using a fast digital data acquisition system. Ultramicroscopy 8, 327-334.

5. Carlemalm, E., Kellenberger, E. (1982). The reproducible observation of unstained embedded cellular material in thin sections: visualization of an integral membrane by a new mode of imaging for STEM. The EMBO Journal 1, 63-67.

6. Colliex, C. (1984). Electron energy-loss spectroscopy in the electron microscope. In: Advances in Optical and Electron Microscopy, ed. V.E. Cosslett (Academic Press, New York) in press.

7. Colliex, C., Trebbia, P. (1978). Electron energy-loss spectroscopy in the electron microscope: present state of affairs. In: Electron Microscopy 1978 (9th Int. Cong., ed. J.M. Sturgess, Microscopical Society of Canada, Toronto) Vol. 3, pp. 268-279.

8. Crewe, A.V. (1970). The current state of high resolution scanning electron microscopy. Quart. Rev. Biophys. 3, 137-175.

9. Daniels, J., Festenberg, C., Raether, H., Zeppenfeld D. (1970). Optical constants of solids by electron spectroscopy. In: Springer Tracts in Modern Physics (Berlin: Springer Verlag) 54, pp. 77-135.

10. Egerton, R.F. (1975). Inelastic scattering of 80 keV electrons in amorphous carbon. Phil. Mag. 31, 199-215.

11. Egerton, R.F. (1978). Quantitative energy-loss spectroscopy. In: Scanning Electron Micros. 1978; I:133-142.

12. Egerton, R.F. (1979). K-shell ionization cross sections for use in microanalysis. Ultramicroscopy 4, 169-179.

13. Egerton, R.F. (1980). Instrumentation and software for energy-loss microanalysis. In: Scanning Electron Micros. 1980; I:41-52.

14. Egerton, R.F. (1982). Thickness dependence of the STEM ratio image. Ultramicroscopy 10, 297-299.

15. Egerton, R.F. (1984). Parallel-recording systems for electron energy-loss spectroscopy (EELS). J. Electron Micros. Tech. 1, 37-52.

16. Egerton, R.F., Kenway, D., (1979). An acquisition, storage, display and processing system for electron energy-loss spectra. Ultramicroscopy 4, 221-225.

17. Egerton, R.F., Whelan, M.J. (1974). The electron energy loss spectrum and band structure of diamond. Phil. Mag. 30, 739-749.

18. Fiori, C.E., Gibson, C.C., Leapman, R.D. (1980). Electrostatic deflection system for use with an electron energy-loss spectrometer. In: Microbeam Analysis 1980, ed. D.B. Wittry (San Francisco Press, San Francisco.) pp. 225-228.

19. Fiori, C.E., Gorlen, K.E., Gibson, C.C. (1981). Comments on the computerization of an analytical electron microscope. 39th Ann. Proc. Electron. Micros. Soc. Amer., ed. G.W. Bailey, (Claitor's Publishing, Baton Rouge, Louisiana.) pp. 246-249.

20. Gorlen, K.E., Barden, L.K., Del Priore, J.S., Kochhar, A.K., Fiori, C.E., Gibson, C.C., Leapman, R.D. (1982). A data acquisition system for an analytical electron microscope. In: Proc. Digital Equipment Computer User Society (USA), Fall 1982, (DECUS, Marlborough, MA) Vol. 9, pp. 181-187. (See also below.)
Gorlen, K.E., Barden, L.K., Del Priore, J.S., Fiori, C.E., Gibson, C.C., Leapman, R.D. (1984). A computerized analytical electron microscope for elemental imaging. Rev. Sci. Instrum. 55, 912-921.

21. Isaacson, M., Johnson, D. (1975). The microanalysis of light elements using transmitted energy-loss electrons. Ultramicroscopy 1, 33-52.

22. Isaacson, M., Ohtsuki, M. (1981). Scanning transmission electron microscopy of small inhomogeneous particles: applications to ferritin. Scanning Electron Micros. 1981; I:73-80.

23. Jeanguillaume, C., Tencé, M., Trebbia, P., Colliex, C. (1983). Electron energy-loss chemical mapping of low Z elements in biological sections. Scanning Electron Micros. 1983; II: 745-756.

24. Jeanguillaume, C., Trebbia, P., Colliex, C. (1978). About the use of electron energy-loss spectroscopy for chemical mapping of thin foils with high spatial resolution. Ultramicroscopy 3, 237-242.

25. Johnson, D.E., Monson, K.L., Csillag, S., Stern, E.A. (1981). An approach to parallel detection electron energy-loss spectrometry. In: Analytical Electron Microscopy 1981, ed. R.H. Geiss (San Francisco Press, San Francisco.) pp. 205-209.

26. Johnson, D.W., Spence, J.C. (1974). Determination of the single scattering distribution from plural scattering data. J. Phys. D. 7, 771-780.

27. Joy, D.C. (1979). The basic principles of electron energy-loss spectroscopy. In: Introduction to Analytical Electron Microscopy (Plenum Press, New York.) pp. 223-244.

28. Joy, D.C., Maher, D.M. (1981). The quantitation of electron energy-loss spectra. J. Microscopy 124, 37-48.

29. Kokubo, Y., Hardy, W.H. (1982). Digital image processing: a path to better pictures. Ultramicroscopy 8, 277-286.

30. Leapman, R.D., Fiori, C.E., Gorlen, K.E., Gibson, C.C., Swyt, C.R. (1984). Combined elemental and STEM imaging under computer control. Ultramicroscopy 12, 281-292.

31. Leapman, R.D., Gorlen, K.E., Swyt, C.R. (1984). Background subtraction in STEM energy loss mapping 42nd Ann. Proc. Electron Micros. Soc. America., Ed. G.W. Bailey (San Francisco Press, San Francisco.) pp. 568-569.

32. Leapman, R.D., Grunes, L.A., Fejes, P.L., Silcox, J. (1981). Extended core edge fine structure in electron energy loss spectroscopy. In: EXAFS Spectroscopy: Techniques and Applications B.K. Teo and D.C. Joy (Eds.) (Plenum Press, New York) pp. 217-240.

33. Leapman, R.D., Swyt, C.R. (1981). Electron energy-loss spectroscopy under conditions of plural scattering. In: Analytical Electron Microscopy 1981, ed. R.H. Geiss (San Francisco Press, San Francisco.) pp. 164-172.

34. Leapman, R.D., Swyt, C.R. (1983). Electron energy-loss imaging in the STEM: systematic and statistical errors. In: Microbeam Analysis 1983, ed. R. Gooley (San Francisco Press, San Francisco.) pp. 163-167.

35. Ottensmeyer, F.P., Andrew, J.W. (1980). High resolution microanalysis of biological specimens by electron energy loss spectroscopy and by electron spectroscopic imaging. Journal of Ultrastructural Research 72, 336-348.

36. Pun, T., Ellis, J.R. (1983). Statistics of edge areas in quantitative EELS imaging: signal-to-noise ratio and minimum detectable signal. In: Microbeam Analysis 1983, ed. R. Gooley (San Francisco Press, San Francisco.) pp. 156-162.

37. Ray, A.B. (1980). Deconvolution of multiple scattering effects from core-level electron energy-loss spectra. 38th Ann. Proc. Electron Micros. Soc. America., Ed., G.W. Bailey (Claitor's Publishing, Baton Rouge, Louisiana.) pp. 522-523.

38. Rez, P., Ahn, C. (1982). Computer control for x-ray and energy-loss line profiles and images. Ultramicroscopy 8, 341-350.

39. Rust, H.P., Krahl, D. (1982). On-line recording and processing of CTEM Images. Ultramicroscopy 8, 287-292.

40. Shuman, H. (1981). Parallel recording of electron energy-loss spectra. Ultramicroscopy 6, 385-396.

41. Shuman, H., Kruit, P., Somlyo, A.P. (1983). Quantitative electron energy-loss spectroscopy of low concentrations of calcium in carbon containing materials. In: Microbeam analysis 1983, ed. R. Gooley (San Francisco Press, San Francisco.) pp. 247-251.

42. Shuman, H., Somlyo, A.P. (1982). Energy-filtered transmission electron microscopy of ferritin. Proc. Natl. Acad. Sci. USA 79, 106-107.

43. Statham, P.J. (1982). Interfacing of computers to a STEM. Ultramicroscopy 8, 309-320.

44. Swyt, C.R., Leapman, R.D. (1982). Plural scattering in electron energy-loss (EELS) microanalysis. In: Scanning Electron Micros. 1982; I:73-82.

Discussion with reviewers

R.F. Egerton: Surely the on-line (analogue) and off-line (digital) methods of forming a "Z-contrast" image are not mutually exclusive? I wonder if it wouldn't be useful to employ a ratio amplifier to display the elastic/inelastic signal in real time, and to use the more accurate and flexible digital techniques (which can be time-consuming without an array processor) only if the display looked promising.

Authors: We agree that analogue and digital methods for Z-contrast imaging are not mutually exclusive and there may be an advantage in a "real-time" display to survey the sample. On the other hand digital acquisition of both signals simultaneously permits a direct and quantitative comparison of the ratio image with the individual elastic and inelastic images. In our system a ratio of two 512 x 512 images can be obtained in about 5 seconds. When frame store display systems with built-in array processors become widely available, it may be anticipated that the digital method will not be more time consuming than the analogue method.

C. Colliex: Can you give more information about the practical conditions of recording characteristic images, in Figs. 8 and 9 for instance? That is: what is a typical probe size and incremental probe step? On Fig. 9, can you tell the number of counts per channel in a typical energy loss image and in the processed characteristic images?

Authors: The probe diameter used to obtain the elemental maps in Fig. 8 was about 20 nm and the incremental probe step was 15 nm. The minimum probe diameter is limited by the available current and 5-10 nm represents the smallest useful probe size in the present system. A field emission source reduces the useful probe size down to the 1 nm level as has been demonstrated by Jeanguillaume et al. [refs. 23 and 24]. In general the probe diameter should be greater than the pixel separation otherwise the image will be undersampled. To image aluminum in Fig. 8 approximately 2000 counts were accumulated in 3 ms at each of ten channels around the aluminum K edge. The spectrometer slit was opened up to about 20 eV to maximize the signal and an average of 6000 counts per pixel was recorded in the processed aluminum K edge image in Fig. 8. In Fig. 9 the energy loss data were obtained only across one line in the sample. Approximately 15000 counts were recorded in 20 ms at each of ten channels around the calcium L_{23} edge. The spectrometer slit width was set at about 5 eV and an average of 5000 counts per pixel was recorded in the processed line profile. The mean number of counts for nitrogen was about the same.

C. Colliex: In fig. 10, how must we use the displayed intensity histograms to learn about the relative concentration of elements in different phases?

Authors: The relative concentrations of elements in different phases can be estimated by finding the position of peaks in the intensity histogram. This requires a knowledge of the zero intensity levels, which are indicated in Fig. 10. For an accurate determination of relative elemental concentrations in the different phases, plural scattering should be taken into account, requiring division of the image in Fig. 10 by the zero-loss image. In this example, the correction for plural scattering was relatively small and was therefore neglected.

C. Colliex: In the last part of the manuscript concerning quantitative EELS mapping, can you comment about your assertion: "it is possible to predict under what circumstances the one-parameter fit should fail, by considering the relative magnitudes of systematic and statistical errors in the spectrum"? The meaning of Eq. (5) and its application to Fig. 11 do not seem to me very obvious when explained in such a short paragraph.

P.E. Batson: Is the one parameter fit for the EELS background often a good approximation, or is it useful only occasionally?

Authors: Detection limits in EELS imaging depend both on statistical and systematic errors. Most of the statistical error arises from the background extrapolation if two parameters (eg. AE^{-r}) are used for fitting. If only one parameter is used for the background. (eg. a simple subtraction of the pre-edge intensity from the post-edge intensity), the statistical error is reduced by as much as a factor of five. This is discussed by R.F. Egerton ("A revised expression for signal/noise in EELS", Ultramicroscopy, 9, (1982) 387-390). The reduction

in noise occurs because the shape of the spectrum (r) is constrained to be invariant. This constraint, however, gives rise to systematic errors in the background subtraction, since changes in shape do in fact occur due to compositional variations and plural scattering effects. The systematic errors in estimated background can be written in terms of these systematic variations in r. Let $\bar{r}$ be the mean value of r for the entire image which is used in a one-parameter fit. Then the new value of A that is needed to fit a curve of the form $A'E^{-\bar{r}}$ through the pre-edge fitting window is given by Eq. (5). If we know *a priori* that r is constant because the composition and mass thickness of the sample are sufficiently uniform, then a one-parameter fit is clearly an advantage because detection limits are reduced. However if the maximum expected systematic error is larger than the statistical error, then artifacts can be produced and a two-parameter fit of form AE^{-r} would be advantageous. In our experience a one-parameter fit is not generally satisfactory except in special cases such as low counting rates or highly uniform sample composition. A criterion for the maximum allowed systematic fluctuations in r for a one-parameter fit, can be obtained by equating expressions for the statistical and systematic errors.

P.E. Batson: What is the day to day accuracy of the EELS energy loss calibration? a) with the magnetic field scanning? b) with the electrostatic scanning?

Authors: In both scanning methods the energy loss per channel remains constant to within about 1 part in 1000, which is sufficient for the applications studied till now in our system. Large offsets (hundreds of eV) are experienced from day to day and these may be due to mechanical movements of the spectrometer, shifts in high voltage or spectrometer supplies, and static fields. These variations do not cause difficulty however in our system. If the spectrum were scanned by offsetting the drift tube electrostatically, the calibration should be constant to within the accuracy of the voltage supply.

P.E. Batson: Please comment on the suspected sources of the 1-2 eV per minute spectrum drift.

Authors: Possible sources are: drift of the high voltage due to thermal effects, drift of the current supply to the spectrometer coils, temperature changes in the spectrometer and changing stray magnetic fields. The precise cause has not been determined yet.

P.E. Batson: What was the approximate time (man years) for the hardware and software development in your lab?

Authors: A total of about 16 man-years was spent developing the system and about 80% of this involved software. Additional effort was involved in experimental work optimizing energy loss and energy dispersive x-ray spectroscopy and in writing applications software.

P.E. Batson: How much care is required in the picking of integration windows for the elemental maps? In your opinion, could your system be marketed commercially for the non-expert?

Authors: Considerable care is needed to choose integration windows in order to (i) avoid overlapping edges (ii) optimize statistical and systematic errors (iii) avoid solid state effects if quantitative measurements are required. Care must also be taken to choose optimum fitting windows for the background in order to avoid regions where the background does not obey a simple power law, and again to optimize statistical and systematic errors. It would be desirable to modernize the hardware if the system were to be made more widely available. Our system might be usable by a non-expert but a certain minimum amount of experience would be necessary to optimize collection of elemental images and to avoid pit-falls leading to artifacts.

D.E. Johnson: Could the authors estimate with calculations and/or experimental results, the minimum detectable concentration obtainable for a typical element, recording time and spatial resolution in an energy loss map? What restrictions on specimen mass thickness (both in average and in spatial variation) are necessary?

Authors: The minimum concentration in an energy loss map depends very strongly on the element and the matrix in which it occurs. As an example, let us consider detection of nitrogen in a carbon matrix, 50 nm thick, containing 3000 carbon atoms per square nanometer. The probe diameter (resolution) depends on the type of electron source used and could be typically between 1 nm and 10 nm; minimum detectable masses will therefore vary accordingly. We can estimate the minimum detectable atomic fraction, however, by making use of cross sections given in ref. [12] for the background due to the carbon K shell at the nitrogen K edge, and the cross section for nitrogen K shell excitation at threshold. Assuming a beam current of 1 nA, a beam energy of 100 keV and a collection semiangle of 10 mrad, we estimate that there are $5 \cdot 10^4$ counts per eV per second in the background and $10^5 x$ counts per eV per second in the nitrogen K edge, where x is the atomic fraction N/C. Consider an image with 128 x 128 pixels recorded in 1000 seconds (60 ms per pixel). In order to record two background channels and one signal channel in series, a counting time per channel of 20 ms is required. Let us assume the spectrometer slit is opened up to 10 eV, then 10^4 counts will be accumulated in each background channel and $2 \cdot 10^4 x$ counts in the nitrogen signal. Using a two-parameter background fit, we estimate a standard deviation in the background estimation of approximately 400 counts (R.F. Egerton, Ultramicroscopy 9 (1982) 387-390). Therefore x is 0.02 for a signal/noise of unity. This represents the approximate detection limit under the above experimental conditions for sample we have chosen, and this figure is also consistent with experimental observations. We have of course neglected mass loss due to radiation damage in this particular example. We also note that an object can be detected with a signal/noise near unity with a resolution of a few pixels in an image since the observer is able to integrate information. For a single point the observer would need a signal/noise of about three for reasonable confidence of detection. If the sample thickness increases, detection limits deteriorate as a result of plural

scattering, which increases the background relative to the signal. In general the sample thickness should be less than the inelastic mean free path, typically 50-100 nm for biological samples at 100 keV beam energy. It is also an advantage for the spatial variation of mass thickness to be small, otherwise systematic errors in the background extrapolation may occur even in a two-parameter fit.

D.E. Johnson: The "concentrations" the authors describe are in terms of projected density (e.g., atoms/cm^2). In a specimen of spatially varying mass thickness, how do you measure true concentration (e.g., atoms/cm^3 or weight fractions?
Authors: In a specimen of spatially varying mass thickness, concentrations may be obtained by forming a ratio of a core edge image with another image that reflects total mass. In a biological sample, carbon represents much of the total mass, and therefore a ratio of one elemental map to the carbon K map may be useful. It is necessary to multiply the quotient by the inverse ratio of their respective cross sections. This method has the advantage of correcting to first order effects of plural scattering. Alternatively, another determination of total mass such as that obtained from the plasmon/zero-loss ratio could be used instead of the carbon K map.

D.E. Johnson: In a typical energy loss image, what would be the range of r values over the image? Do you correlate the spread in r values with the minimum detectable concentrations?
Authors: The range of r values depends very strongly on the region of the spectrum and the number of counts accumulated at each pixel. The range decreases as the fitting window for the background increases. In the calcium map shown in Fig. 11, the distribution of r had a standard deviation of 0.27, a mean of 2.6 and a range extending from 1.5 to 3.5. It would be interesting to correlate directly the spread in r with the minimum detectable concentrations but we have not done this yet. One would need to distinguish between spread in r due to statistical fluctuations in the fitting region, and spread in r due to systematic differences in spectral shape, however.